European Journal of Wood and Wood Products
Volume 75, Issue 6, pp 973–983 (2017)

Cross Laminated Timber Properties Including Effects of Non-Glued Edges and Additional Cracks

John A. Nairn

Received: 19 January 2017; Published November 2017: DOI 10.1007/s00107-017-1202-y

Abstract Cross laminated timber (CLT) is usually comprised of multiple timber layers having alternating grain directions. Because individual boards are glued on their faces between layers, but usually not glued on their edges within layers, those edges define "precracks" in the composite. When exposed to differential thermal and moisture expansion after installation, CLT, like all cross-laminated composites, is prone to formation of "additional cracks." Confidant CLT design must be able to account for changes in CLT properties during life of a structure caused by such additional cracks. By extending variational mechanics methods for aerospace composites, this paper provides analytical solutions for all in-plane mechanical, thermal expansion, and moisture expansion properties of a three-layer CLT panel. By using the three-layer solution to evaluate effective layer properties as a function of the number of cracks, the analysis can be extended to in-plane mechanical, out-of-plane bending, and expansion properties for CLT panels with any number or arrangement of layers. Some sample calculations are provided along with comments on limitations of the approximations and needs for future work.

1 Introduction

Cross laminated timber (CLT) is usually made by laminating three or more timber layers such that grain directions in alternate layers are at right angles to each other. Glue is applied between the layers on timber faces, but, most commonly, no glue is applied on timber edges within layers. In other words, CLT is a precracked composite where timber edges represent periodic "precracks." Furthermore, CLT will develop "additional cracks" over time due to environmental exposure and differential layer shrinkages. This fact is known from observed cracks within installed CLT (Nairn, 2016b) and is expected from experiments on cracking of layers in other cross-laminated structures (Nairn and Hu, 1994; Nairn, 2000). Prior work also shows that added cracks form more easily as layer thickness increases (Parvizi et al, 1978; Nairn, 1989). In other words, the use of thick timber in CLT unfortunately promotes cracking compared to cross-laminated panels with more, but thinner layers. Attempts to ameliorate effects of precracks by applying glue to edges would be thwarted by natural formation of added cracks over time. The inescapable conclusions are that CLT structures must be designed with tools that recognize cracks and durability analysis of CLT must account for the rate of formation of added cracks and their role in changing structural properties.

Fortunately, most of the methods needed for CLT analysis with cracks are already available from prior research on synthetic-material, cross-ply laminates (Hashin, 1985, 1986, 1987, 1988; Nairn, 1989). Applications of synthetic cross-ply laminates include aerospace structures, bicycle tubes, ski poles, filament wound pressure vessels, and fiberglass pipes (the last two are not exactly cross laminated, but are close). Unlike CLT, synthetic cross-ply laminates are not manufactured with precracks, but like CLT, such laminates are prone to added cracks (referred to in the literature as "microcracks" or "transverse cracks") caused by mechanical loads or by residual stresses (see reviews in (Nairn

John A. Nairn
Oregon State University, Wood Science & Engineering
112 Richardson Hall, Corvallis, OR 97330, USA
Tel.: +1-541-737-4265, Fax: +1-541-737-3385, E-mail: John.Nairn@oregonstate.edu

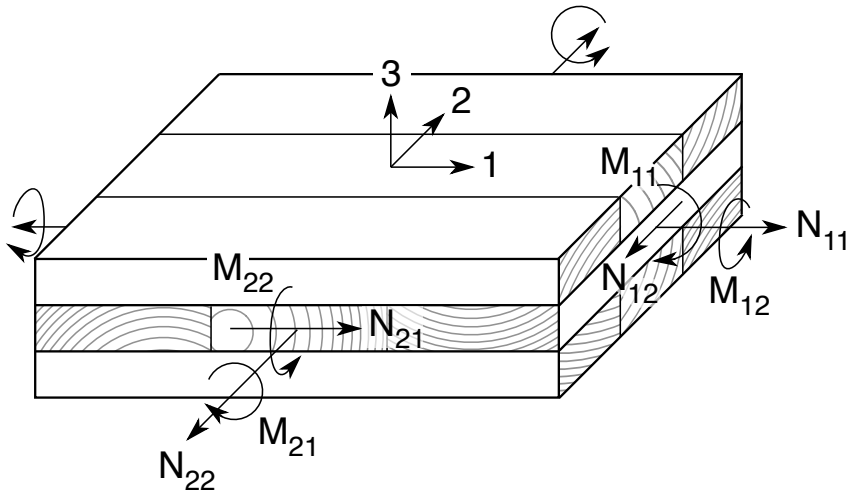

Fig. 1 A three-layer CLT panel showing force (N) and moment (M) resultants for laminated plate theory and showing the 1-2-3 laminate axis system.

and Hu, 1994; Nairn, 2000)). The consequences of microcracks are a reduction in laminate properties, a promotion of more serious damage such as delamination, or the possibility of leakage in pressure vessels or pipes (Frost, 1994).

This paper extends prior composite models to find all mechanical and expansion (thermal or moisture) properties of CLT panels with cracked layers. Although most prior microcracking models are 2D models for cracking in a single layer, Hashin (Hashin, 1987) analyzed a three-layer, orthogonally-cracked, cross-laminated composite, which is an exact analog of a three-layer CLT panel. He found in-plane tensile modulus in one direction and Poisson's ratio. This work extends his analysis to orthotropic wood layers, finds tensile moduli in both directions, corrects an error in his Poisson's ratio calculation, finds thermal and moisture expansion coefficients, and adapts a different method to find shear modulus. All properties are found as a function of crack density. To extend the calculations to any number of layers, the three-layer solution was used to deduce *effective* properties for an isolated layer containing cracks. These effective properties can then be used in conventional laminate analysis to find in-plane, bending, and expansion properties of any CLT panel. Sample calculations are presented along with discussion of the consequence of cracks, limitations of the methods, and needs for future modeling and experiments.

2 Alternative-Layer CLT Property Analysis

2.1 Baseline Properties

Step one is to find properties in a panel with no cracks, which must be recognized as upper bound properties that are never realized in real panels. A three-layer CLT panel together with in-plane and moment loads is shown in Fig. 1. A general CLT panel has n alternating 0° and 90° layers with 0° layers on both surfaces (thus $(n+1)/2$ 0° layers, $(n-1)/2$ 90° layers, where n is odd). The panel 1 direction is grain direction in the 0° layers while the 2 direction is grain direction in the 90° layers. All layers are assumed to have the same thickness and the same grade of timber. Such a structure's properties are easily found from laminated plate theory (LPT). LPT details are in many text books (Christenson, 1979; Jones, 1975); Appendix 1 has minimal, yet complete, methods specialized for symmetric, cross-laminated plates.

All baseline, in-plane properties for an n-layer CLT are found from LPT (see Appendix 1) using:

$$\begin{array}{ccc} \nu_{12}^0 = \frac{2nR\nu_{Lt}}{(n-1)+R(n+1)} & & \nu_{21}^0 = \frac{2nR\nu_{Lt}}{(n+1)+R(n-1)} \\ E_{11}^0 = \frac{E_L R\nu_{Lt}}{\nu_{21}^0(1-R\nu_{Lt}^2)}(1-\nu_{12}^0\nu_{21}^0) & G_{12}^0 = G_{Lt} & E_{22}^0 = \frac{E_L R\nu_{Lt}}{\nu_{12}^0(1-R\nu_{Lt}^2)}(1-\nu_{12}^0\nu_{21}^0) \end{array} \tag{1}$$

Here E_L and G_{Lt} are tensile and shear moduli of the timber layers parallel to the grain, ν_{Lt} is the axial Poisson's ratio, and $R = E_t/E_L$ is ratio of tensile moduli in transverse and grain directions of the timber. Note that the lowercase "t" in

E_t, G_{Lt}, and ν_{Lt} means "transverse" direction in the board and not the "tangential" direction in wood. The actual value for E_t depends on the timber's end-grain pattern. For flat-sawn boards, $t \approx T$ and $r \approx R$ (where r means thickness direction of the board). but, for radially sawn boards, $t \approx R$ and $r \approx T$. For off-axis end-grain patterns, E_t and E_r may assume other values including potentially lower than both E_R and E_T (Nairn, 2007). Here E_t is assumed the same for all layers (but it could easily be varied in calculations to assess end-grain pattern effects).

2.2 Variational Mechanics for In-Plane Normal Stresses

Step two is to find effective properties relative to reference properties as a function of the number of cracks in the layers. Analysis of cracked, cross laminated composites has a long history with the most accurate, analytical methods being derived using variational mechanics (Hashin, 1985). Although most prior work was 2D, Hashin derived a 3D variational mechanics approach to analyze a cross laminated composite with orthogonal cracks in all layers (Hashin, 1987), which is equivalent to the CLT structure in Fig. 1. Hashin considered only tensile loading in the 1 direction and treated the layers as transversely isotopic materials. For use in CLT, his approach must be extended to handle loading in both directions and to allow full orthotropic properties for wood. Fortunately, these extensions are mostly straightforward. This section outlines the revised analysis emphasizing differences from Hashin's analysis and corrects one error in his analysis for Poisson's ratio.

Figures 2A and B show analysis coordinates for a single unit cell between cracks (indicated as shaded areas) in the layers for loading in both the 1 (from Hashin) and 2 (added here) directions. To maximize overlap with Hashin's analysis, the direction 2 analysis rotates the materials 90° about the z axis. Each problem considers one half by symmetry defined by $0 \le z \le h$ with $-a \le x \le a$ and $-b \le y \le b$ for direction 1, but $-b \le x \le b$ and $-a \le y \le a$ for direction 2. Note that the z axis for direction 2 is shifted by $h/2$. With this shift, the layers labeled (1) and (2) have the same orthotropic wood properties — *x*-*y*-*z* directions in *t*-*L*-*r* directions for layer (1) and *L*-*t*-*r* direction for layer (2) – and have cracks on the same surfaces. A difference between directions 1 and 2 is that $z = 0$ and $z = h$ are midplane of symmetry and free surface, respectively, for direction 1 while they are the opposite for direction 2. When the cracks are timber edges, crack spacings ($2a$ and $2b$) are timber widths in those layers. Most CLT has layers of the same thickness ($2t_1 = t_2$) and same size timber ($2a = 2b$), but they are left as independent variables to keep the analysis more general.

Hashin (1987) wrote total stress in layer (k) as:

$$\sigma_{ij}^{(k,tot)} = \sigma_{ij}^{(k,0)} + \sigma_{ij}^{(k)} \tag{2}$$

where $\sigma_{ij}^{(k,0)}$ is stress in a panel with no cracks and $\sigma_{ij}^{(k)}$ is a perturbation stress or change in stress due to cracks. He derived a 3D admissible, perturbation stress state for each layer, which was extended here to account for both loading directions ($i = 1$ or 2), as

$$\begin{array}{llll} \sigma_{xx}^{(1)} = -\sigma_0 k_{xi}\phi_i(x) & \sigma_{xx}^{(2)} = \frac{1}{\lambda_i}\sigma_0 k_{xi}\phi_i(x) & \sigma_{xy}^{(1)} = 0 & \sigma_{xy}^{(2)} = 0 \\ \sigma_{yy}^{(1)} = -\sigma_0 k_{yi}\psi_i(y) & \sigma_{yy}^{(2)} = \frac{1}{\lambda_i}\sigma_0 k_{yi}\psi_i(y) & \sigma_{xz}^{(1)} = \sigma_0 k_{xi}\phi_i'(x)z & \sigma_{xz}^{(2)} = \frac{1}{\lambda_i}\sigma_0 k_{xi}\phi_i'(x)(h-z) \end{array} \tag{3}$$

$$\sigma_{yz}^{(1)} = \sigma_0 k_{yi}\psi_i'(y)z \qquad \sigma_{zz}^{(1)} = \begin{cases} \sigma_0\left[k_{xi}\phi_1''(x) + k_{yi}\psi_1''(y)\right]\frac{1}{2}(ht_1 - z^2) & \text{direction 1} \\ -\sigma_0\left[k_{xi}\phi_2''(x) + k_{yi}\psi_2''(y)\right]\frac{1}{2}z^2 & \text{direction 2} \end{cases} \tag{4}$$

$$\sigma_{yz}^{(2)} = \frac{1}{\lambda_i}\sigma_0 k_{yi}\psi_i'(y)(h-z) \qquad \sigma_{zz}^{(2)} = \begin{cases} \sigma_0\left[k_{xi}\phi_1''(x) + k_{yi}\psi_1''(y)\right]\frac{1}{2\lambda_i}(h-z)^2 & \text{direction 1} \\ \sigma_0\left[k_{xi}\phi_2''(x) + k_{yi}\psi_2''(y)\right]\frac{1}{2\lambda_i}\left(h(t_2-2z)+z^2\right) & \text{direction 2} \end{cases} \tag{5}$$

where $\phi_i(x)$ and $\psi_i(y)$ are four unknown functions (two for each loading direction), $\lambda_1 = t_2/t_1$, and $\lambda_2 = t_1/t_2$. The stiffnesses, k_{xi} and k_{yi}, give the stress in layer 1 of the uncracked laminate due to uniaxial load in direction i and are easily calculated from LPT. The only non-zero initial stresses are:

$$\sigma_{xx}^{(1,0)} = k_{xi}\sigma_0 \qquad \text{and} \qquad \sigma_{yy}^{(1,0)} = k_{yi}\sigma_0 \tag{6}$$

where

$$k_{xi} = \begin{cases} \frac{RE_L(1-\nu_{Lt}\nu_{12}^0)}{E_{11}^0(1-R\nu_{Lt}^2)} & \text{for } i = 1 \\ \frac{RE_L(1-\nu_{Lt}\nu_{21}^0)}{E_{22}^0(1-R\nu_{Lt}^2)} & \text{for } i = 2 \end{cases} \qquad \text{and} \qquad k_{yi} = \begin{cases} \frac{E_L(R\nu_{Lt}-\nu_{12}^0)}{E_{11}^0(1-R\nu_{Lt}^2)} & \text{for } i = 1 \\ \frac{E_L(R\nu_{Lt}-\nu_{21}^0)}{E_{22}^0(1-R\nu_{Lt}^2)} & \text{for } i = 2 \end{cases} \tag{7}$$

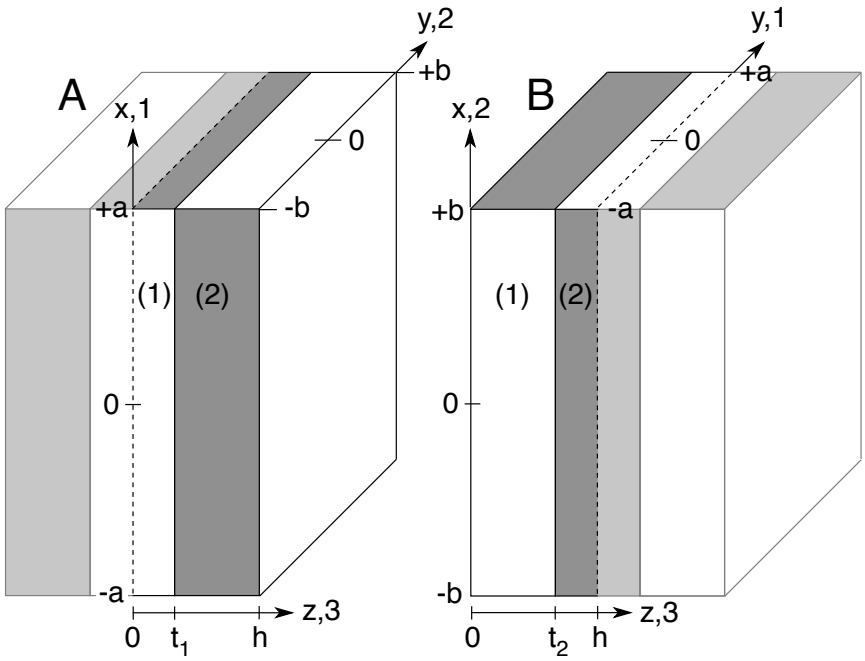

Fig. 2 Unit cells for analysis three-layer CLT panels for loading in the 1 or 2 directions. The unit cell boundaries are defined by crack surfaces indicated as shaded areas. The *x*-*y*-*z* coordinates are the same in the two unit cells, but the laminated axes are rotated 90° for the direction 2 analysis.

The simplifying assumption of these stress states is that normal stresses are independent of thickness within the layers although they do depend on distance from the cracks. Otherwise, the stress states are valid admissible stress states. They satisfies all 3D equilibrium conditions, have zero shear on free surfaces and on midplanes of symmetry ($\sigma_{xz}^{(1)}(z=0)=0$, $\sigma_{xz}^{(2)}(z=h)=0$, $\sigma_{yz}^{(1)}(z=0)=0$, and $\sigma_{yz}^{(2)}(z=h)=0$), have zero normal stress on free surfaces ($\sigma_{zz}^{(2)}(z=h)=0$ for 1 direction and $\sigma_{zz}^{(1)}(z=0)=0$ for 2 direction), and satisfies continuity of σ_{zz}, σ_{xz}, and σ_{yz} at the layer interface. Finally, the stresses satisfy all traction boundary conditions provided the unknown functions satisfy:

$$\phi_1(\pm a)=\psi_1(\pm b)=1,\quad \phi_1'(\pm a)=\psi_1'(\pm b)=0,\quad \phi_2(\pm b)=\psi_2(\pm a)=1,\quad \text{and}\quad \phi_2'(\pm b)=\psi_2'(\pm a)=0 \tag{8}$$

These values result in zero normal and shear stress on all crack surfaces.

By variational mechanics, the lower-bound modulus in the presence of crack spacings a and b in one loading direction ($i=1$ or 2) is:

$$\frac{1}{E_{ii}(a,b)} \le \frac{1}{E_{ii}^0} + \frac{2U_{ci}}{V\sigma_0^2} \tag{9}$$

where V is total volume, σ_0 is uniaxial stress in direction i, and U_{ci} is complementary energy calculated from perturbation stresses alone:

$$U_{ci} = \frac{1}{2}\int \sigma\cdot \mathsf{S}\sigma\, dV \tag{10}$$

Here S is the position-dependent compliance tensor (note: the simplification to consider only perturbation stresses in the energy analysis follows from Hashin's proof that complementary energy of any cracked body is sum of U_{ci} from perturbation stress and U_{ci}^0 from stresses in the uncracked body (Hashin, 1987)). The remaining task is to find U_{ci} by using variational calculus to find the unknown $\phi_i(x)$ and $\psi_i(y)$ functions that minimize complementary energy.

Differing from Hashin, CLT layers are orthotropic instead of transversely isotropic. The local stress energy density in layers (1) and (2) become:

$$2W^{(1)} = \frac{{\sigma_{xx}^{(1)}}^2}{E_t} + \frac{{\sigma_{yy}^{(1)}}^2}{E_L} + \frac{{\sigma_{zz}^{(1)}}^2}{E_r} - \frac{2\sigma_{yy}^{(1)}(\nu_{Lt}\sigma_{xx}^{(1)}+\nu_{Lr}\sigma_{zz}^{(1)})}{E_L} - \frac{2\nu_{tr}\sigma_{xx}^{(1)}\sigma_{zz}^{(1)}}{E_t} + \frac{{\sigma_{yz}^{(1)}}^2}{G_{Lr}} + \frac{{\sigma_{xz}^{(1)}}^2}{G_{RS}} \tag{11}$$

$$2W^{(2)} = \frac{{\sigma_{xx}^{(2)}}^2}{E_L} + \frac{{\sigma_{yy}^{(2)}}^2}{E_t} + \frac{{\sigma_{zz}^{(2)}}^2}{E_r} - \frac{2\sigma_{xx}^{(2)}(\nu_{Lt}\sigma_{yy}^{(1)} + \nu_{Lr}\sigma_{zz}^{(2)})}{E_L} - \frac{2\nu_{tr}\sigma_{yy}^{(2)}\sigma_{zz}^{(2)}}{E_t} + \frac{{\sigma_{yz}^{(2)}}^2}{G_{RS}} + \frac{{\sigma_{xz}^{(2)}}^2}{G_{Lr}} \tag{12}$$

Recall that L is longitudinal direction, but t and r refer to transverse and thickness directions of the boards, which will refer to different wood directions depending on end-grain orientation (as discussed above). G_{RS} is the rolling shear modulus for wood in the transverse plane. It is likely less dependent on grain pattern and given here as a fixed value. G_{RS}, however, may be very low due to the cellular structure of wood (Gibson and Ashby, 1997).

The complementary energy of the unit cell for loading direction i is:

$$U_{ci} = t_i^2 \int_{-\rho_i}^{\rho_i} \int_{-\chi_i}^{\chi_i} \left(\int_0^{t_1} W^{(1)}\, dz + \int_{t_1}^{h} W^{(2)}\, dz \right) d\eta\, d\xi \tag{13}$$

where $\xi = x/t_i$ and $\eta = y/t_i$ are dimensionless coordinates and $\rho_1 = a/t_1$, $\rho_2 = b/t_2$, $\chi_1 = b/t_1$, and $\chi_2 = a/t_2$ are dimensionless crack spacings for x and y axes. Inserting stresses and integrating over z, the complementary energy is

$$\begin{aligned} 2U_{ci} = \sigma_0^2 t_i^3 \int_{-\rho_i}^{\rho_i} \int_{-\chi_i}^{\chi_i} \big(& A_0 {k_{xi}}^2 \phi^2 + 2B_0 k_{xi} k_{yi} \phi\, \psi + C_0 {k_{yi}}^2 \psi^2 + A_1 {k_{xi}}^2 \phi'^2 + B_1 {k_{yi}}^2 \psi'^2 \\ & + A_2 k_{xi} \phi (k_{xi}\phi'' + k_{yi}\psi'') + B_2 k_{yi} \psi (k_{xi}\phi'' + k_{yi}\psi'') + C_2 (k_{xi}\phi'' + k_{yi}\psi'')^2 \big) d\xi\, d\eta \end{aligned} \tag{14}$$

where $\phi = \phi_i(\xi)$ and $\psi = \psi_i(\eta)$. This result is identical to analysis in (Hashin, 1987) but has new constants to represent wood properties and two sets of constants are needed to solve the separate problems for loading in the 1 or the 2 direction. The constants relevant for loading CLT in the $i = 1$ direction are:

$$\begin{array}{ccc} A_0 = \frac{1}{E_t} + \frac{1}{\lambda_i E_L} & B_0 = -\frac{\nu_{Lt}(1+\lambda_i)}{\lambda_i E_L} & C_0 = \frac{1}{E_L} + \frac{1}{\lambda_i E_t} \\ A_1 = \frac{1}{3G_{RS}} + \frac{\lambda_i}{3G_{Lr}} & B_1 = \frac{1}{3G_{Lr}} + \frac{\lambda_i}{3G_{RS}} & A_2 = \frac{(3\lambda_1+2)\nu_{tr}}{3E_t} - \frac{\lambda_1 \nu_{Lr}}{3E_L} \\ B_2 = \frac{(3\lambda_1+2)\nu_{Lr}}{3E_L} - \frac{\lambda_1 \nu_{tr}}{3E_t} & C_2 = \frac{(\lambda_1+1)(3\lambda_1^2+12\lambda_1+8)}{60E_r} & \end{array} \tag{15}$$

For loading in the $i = 2$ direction, the last three constants are replaced by:

$$A_2' = \frac{(2\lambda_2+3)\nu_{Lr}}{3E_L} - \frac{\nu_{tr}}{3E_t} \quad B_2' = \frac{(2\lambda_2+3)\nu_{tr}}{3E_t} - \frac{\nu_{Lr}}{3E_L} \quad C_2' = \frac{(\lambda_2+1)(8\lambda_2^2+12\lambda_2+3)}{60E_r} \tag{16}$$

The next steps use calculus of variations to solve two coupled differential equations for $\phi_i(x)$ and $\psi_i(y)$, substitute those solutions into Eq. 14 to find U_{ci}, and finally use Eq. 9 to find modulus. Because Eq. (14) is identical to the (Hashin, 1987) analysis, except for revised constants in Eqs. (15) and (16), the solution process is also identical and need not be repeated. Applying Hashin's solution to CLT loading in each direction, lower bounds on the two tensile moduli are:

$$\frac{1}{E_{11}(a,b)} \le \frac{1}{E_{11}^0} + \frac{1}{1+\lambda_1} \left(K_{x1} \langle \phi_1 \rangle + K_{y1} \langle \psi_1 \rangle \right) \tag{17}$$

$$\frac{1}{E_{22}(a,b)} \le \frac{1}{E_{22}^0} + \frac{1}{1+\lambda_2} \left(K_{x2} \langle \phi_2 \rangle + K_{y2} \langle \psi_2 \rangle \right) \tag{18}$$

where

$$K_{xi} = k_{xi} \left(\frac{k_{xi}(\lambda_i E_L + E_t) - k_{yi} E_t \nu_{Lt}(1+\lambda_i)}{\lambda_i E_L E_t} \right), \qquad K_{yi} = k_{yi} \left(\frac{k_{yi}(E_L + \lambda_i E_t) - k_{xi} E_t \nu_{Lt}(1+\lambda_i)}{\lambda_i E_L E_t} \right) \tag{19}$$

and $\langle \phi_i \rangle$ and $\langle \psi_i \rangle$ are average values of the solved functions for loading direction i. Explicit solutions for these average values are given in Hashin (1987) and in Appendix 2. These moduli assume all unit cells in a CLT panel have the same wood properties. The equations are easily adapted to account for expected variations in timber properties by averaging a collection of unit cells having a given probability distribution of wood properties.

Although Poisson ratios cannot be bounded, they can be calculated from the stress state found in the process of energy minimization. For direction 1 loading

$$\frac{\nu_{12}(a,b)}{E_{11}(a,b)} = -\frac{\langle \varepsilon_{22} \rangle}{\sigma_0} \tag{20}$$

where $\langle\varepsilon_{22}\rangle$ is average apparent strain in the 2 direction. Hashin mistakenly equated this strain to

$$\left\langle\varepsilon_{22}^{(0)}\right\rangle = \frac{1}{h}\left(t_1\overline{\varepsilon_{yy}^{(1)}} + t_2\overline{\varepsilon_{yy}^{(2)}}\right) \tag{21}$$

where $\overline{\varepsilon_{yy}^{(i)}}$ is strain averaged over that phase volume. But this calculation does not account for extra strain resulting from crack opening displacements. For layer 2, the average crack opening displacement can be found from difference of strains in the two layers:

$$\langle\delta\rangle = 2b\left(\overline{\varepsilon_{yy}^{(1)}} - \overline{\varepsilon_{yy}^{(2)}}\right) \tag{22}$$

Combining this displacement with zero crack opening displacement in layer 1, converting to strain, and expressing as average over the full composite, the average strain due to crack opening displacements is

$$\left\langle\varepsilon_{22}^{(cod)}\right\rangle = \frac{t_2}{h}\left(\overline{\varepsilon_{yy}^{(1)}} - \overline{\varepsilon_{yy}^{(2)}}\right) \tag{23}$$

The total apparent strain needed to find Poisson's ratio simplifies to

$$\langle\varepsilon_{22}\rangle = \left\langle\varepsilon_{22}^{(0)}\right\rangle + \left\langle\varepsilon_{22}^{(cod)}\right\rangle = \overline{\varepsilon_{yy}^{(1)}} \tag{24}$$

Finding $\varepsilon_{yy}^{(1)}$ from total stress (Eqs. (3) to (5)), making use of $\overline{\phi_i''} = \overline{\psi_i''} = 0$, and repeating for both loading directions, leads to:

$$\frac{\nu_{12}(a,b)}{E_{11}(a,b)} = \frac{\nu_{12}^0}{E_{11}^0} + \frac{1}{E_L}\left(k_{y1}\langle\psi_1\rangle - \nu_{Lt}k_{x1}\langle\phi_1\rangle\right) \quad \text{and} \quad \frac{\nu_{21}(a,b)}{E_{22}(a,b)} = \frac{\nu_{21}^0}{E_{22}^0} + \frac{1}{E_L}\left(k_{y2}\langle\psi_2\rangle - \nu_{Lt}k_{x2}\langle\phi_2\rangle\right) \tag{25}$$

2.3 In-Plane Shear Loading

Hashin (1987) mentions that "the problem of shearing of a cross-ply will be considered elsewhere." Unfortunately, the methods used for in-plane axial loading are not easily extended to shear loading. As a result, the 3D shearing problem has not been solved (Hashin, 2010). We can however, build an approximate 3D solution by using an existing 2D solution for in-plane shear modulus of a cracked cross-ply laminate with only one cracked layer (Hashin, 1986).

Figure 3A shows edge view of a CLT panel with cracks only in the middle layer. Hashin derived the in-plane shear modulus for such a laminate, which is a 2D problem (Hashin, 1986). Using wood properties in that analysis, the lower bound shear modulus is:

$$G_{12}(a,\infty) \ge \frac{G_{Lt}}{1+\frac{\tanh(\mu_1 a/t_1)}{\lambda_1\mu_1 a/t_1}} \qquad \text{where} \qquad \mu_1 = \frac{3(1+\lambda_2)}{G_{Lt}\left(\frac{1}{G_{Lr}}+\frac{\lambda_1}{G_{RS}}\right)} \tag{26}$$

Here $G_{12}(a,\infty)$ indicates shear modulus for a panel with cracks only in the middle layer. Figure 3B shows edge view of a CLT panel with cracks only in the surfaces layers. A straight-forward extension of Hashin's approach (or simple inspection by those confident to use that method) leads to:

$$G_{12}(\infty,b) \ge \frac{G_{Lt}}{1+\frac{\tanh(\mu_2 b/t_2)}{\lambda_2\mu_2 b/t_2}} \qquad \text{where} \qquad \mu_2 = \frac{3(1+\lambda_1)}{G_{Lt}\left(\frac{1}{G_{Lr}}+\frac{\lambda_2}{G_{RS}}\right)} \tag{27}$$

For an approximate 3D analysis, we write the above 2D solution for a cracked laminate as:

$$G_{12}(a,\infty) = \frac{t_1 G_{Lt}^*(a,\infty) + t_2 G_{Lt}}{t_1+t_2} \qquad \text{and} \qquad G_{12}(\infty,b) = \frac{t_1 G_{Lt} + t_2 G_{Lt}^*(\infty,b)}{t_1+t_2} \tag{28}$$

The right-hand sides are LPT analyses for shear modulus while $G_{Lt}^*(a,\infty)$ and $G_{Lt}^*(\infty,b)$ are effective shear moduli for cracked middle or surface layers, respectively. Solving for effective properties and then using LPT when all layers are cracked, the shear modulus can be approximated as:

$$G_{12}(a,b) \ge \frac{t_1 G_{Lt}^*(a,\infty) + t_2 G_{Lt}^*(\infty,b)}{t_1+t_2} = G_{12}(a,\infty) + G_{12}(\infty,b) - G_{Lt} \tag{29}$$

or

$$G_{12}(a,b) \ge G_{12}^0 - G_{Lt}\left(\frac{\tanh(\mu_1 a/t_1)}{\tanh(\mu_1 a/t_1)+\lambda_1\mu_1 a/t_1} + \frac{\tanh(\mu_2 b/t_2)}{\tanh(\mu_2 b/t_2)+\lambda_2\mu_2 b/t_2}\right) \tag{30}$$

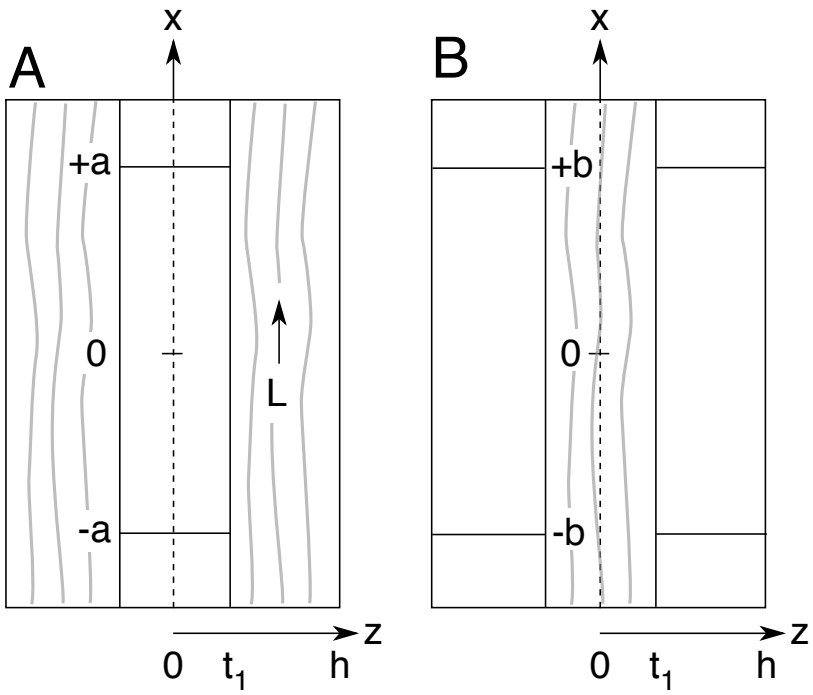

Fig. 3 Unit cells for 2D analysis of in-plane shear modulus for three-layer CLT panel with cracks only in the middle layer (A) or only in the surface layers (B). The longitudinal wood direction in the uncracked layers is in the x direction, but in the cracked layers, it is in the y direction.

2.4 Thermal and Moisture Expansion Coefficients

The usual approach to finding thermal expansion coefficients is to start over with a stress analysis that includes residual stresses, but that work is not needed. Instead, thermal expansion coefficients of a CLT structure can be found from the Levin equation (Levin, 1967):

$$\sigma^{(m)} \cdot \alpha_{eff} = \sum_k V_k \overline{\sigma_k^{(m)}} \cdot \alpha_k \tag{31}$$

where $\sigma^{(m)}$ is any applied mechanical stress, α_{eff} is the CLT expansion tensor, V_k, $\overline{\sigma_k^{(m)}}$, and α_k are volume fraction, average mechanical stress, and expansion coefficients of layer k. Applying this result using the above stress solution for each loading direction i, straightforward calculations lead to

$$\alpha_1(a,b) = \alpha_L + \frac{\alpha_t - \alpha_L}{1+\lambda_1}\big(k_{x1}(1-\langle\phi_1\rangle) - k_{y1}(1-\langle\psi_1\rangle)\big) \tag{32}$$

$$\alpha_2(a,b) = \alpha_L + \frac{\alpha_t - \alpha_L}{1+\lambda_2}\big(k_{x2}(1-\langle\phi_2\rangle) - k_{y2}(1-\langle\psi_2\rangle)\big) \tag{33}$$

where α_L and α_t are longitudinal and transverse thermal expansion coefficients of the timber. Note that CLT expansion coefficients with no cracks (α_1^0 and α_2^0) are found from Eqs. (32) and (33) by setting $\langle\phi_i\rangle = \langle\psi_i\rangle = 0$. This result is, as expected, identical to classical lamination theory approach to thermal expansion coefficients (Christenson, 1979; Jones, 1975). Moisture expansion coefficients, which may be more important for wood products, are found simply by replacing all thermal expansion coefficients (α) with the corresponding moisture expansion coefficients (β) for both the CLT panel and the wood.

Table 1 The mechanical and moisture expansions properties used for the timber in all calculations. The calculations were for flat-sawn timber, which results in transverse (t) and thickness (r) directions of the timber boards being in the tangential (T) and radial (R) directions of the wood.

Property	Value	Property	Value	Property	Value	Property	Value	Property	Value
E_L (GPa)	8.0	E_t (GPa)	0.62	E_r (GPa)	0.96	G_{Lt} (GPa)	0.8	G_{RS} (GPa)	0.08
ν_{Lt}	0.532	ν_{Lr}	0.427	ν_{tr}	0.35	β_L (wt^{-1})	0.0	β_t (wt^{-1})	0.26

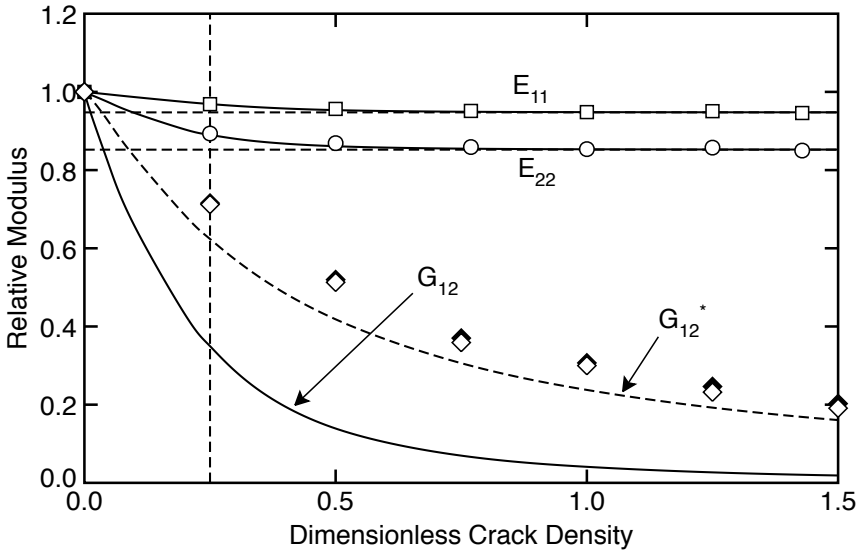

Fig. 4 The axial moduli (E_1 and E_2) and in-plane shear modulus (G_{12}) for a three-layer CLT panel as a function of crack density in the layers. The smooth lines are predictions from variational mechanics. The symbols are 3D MPM results. The filled symbols are 3D MPM results when the crack surfaces contact by friction. The dashed line is a semi-analytical model for G_{12} from Bogensperger et al (2010). All values are normalized to the modulus with no cracks.

3 Results and Discussion

3.1 In-Plane Mechanical Properties

This section gives sample calculations for CLT properties as a function of crack spacings for three-layer CLT made from flat-sawn timber. The initial timber cross section is 40×160 mm (1.57×6.30 in) and identical in all layers leading to $2t_1 = t_2 = 40$ mm and $a = b = 80$ mm. All results are plotted as a function of dimensionless crack density equal to $1/\rho_1 = t_1/a$ where ρ_1 is the aspect ratio of the timber's cross-section. This as-made CLT has $1/\rho_1 = 0.25$ while zero crack density corresponds to CLT with no cracks and $1/\rho_1 > 0.25$ corresponds to changes in properties caused by added cracks. The assumed wood properties are in Table 1; for flat sawn timber t and r in the timber correspond to T and R directions of wood.

The solid curves in Fig. 4 plot in-plane tensile and shear moduli calculated by Eqs. (17), (18), and (30). All results were normalized to moduli for CLT with no cracks. The vertical dashed line marks the crack density for as-made CLT. The tensile moduli decrease as crack density increases. Both E_1 and E_2 approach "ply discount" limits (horizontal dashed lines) that correspond to a calculation that assumes the transverse plies contribute zero stiffness to the panel. Tensile moduli decreases are modest because the E_L/E_T ratio is high for wood. The 90 degree layers never contribute much stiffness and therefore when cracks form, the degradation is rather small. The degradation would be slightly larger for radial-sawn timber (because $E_R > E_T$). The drop in shear modulus is much larger. In fact, CLT shear modulus tends to zero as crack density increases.

The complementary energy analysis for moduli finds lower bounds to those moduli. To check the accuracy of these lower bounds, the symbols show 3D numerical calculations (using the material point method (MPM) (Sulsky et al, 1994; Nairn, 2013, 2016a)). The numerical model for tensile moduli used the unit cell in Fig. 2. The analytical and numerical results agree well demonstrating that the lower bounds are close to actual moduli. Attempts to find

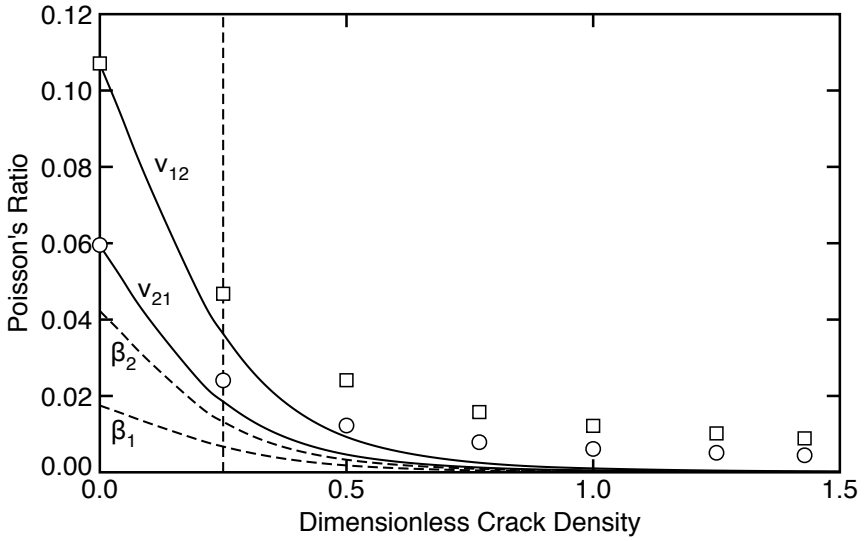

Fig. 5 The Poisson's ratios (ν_{12} and nu_{21}) and the coefficients of moisture expansion (β_1 and β_2) for a three-layer CLT panel as a function of crack density.

shear modulus by considering a single unit cell with shear force applied only to non-cracked surfaces only were unrealistic. An alternate approach was to increase the size of the modeled CLT to include $N \times N$ unit cells and apply uniform shear on edges of the full structure. For large N, this approach is modeling a complete CLT panel. Analysis of multiple unit cells requires numerical methods that can handle sliding at interior non-glued edges but stick conditions on glued faces. Fortunately, MPM can handle this issue (Nairn, 2013). The open symbols in Fig. 4 show shear modulus calculated from an $N \times N$ model with $N = 5$; N was chosen by separate calculations as a function of N that showed converged results for $N \geq 4$. The numerical result decays significantly, but slower than the analytical model. In other words, the variational analysis used for $G_{12}(a,b)$ is a pessimistic lower bound.

An alternate analysis for CLT shear modulus is given in Bogensperger et al (2010). This analysis used many simplifying assumption (*e.g.*, zero stiffness transverse to the plies), is limited to CLT with constant board widths ($2a = 2b$) and constant thickness ($2t_1 = t_2$), and required calibration by 3D finite element modeling. The semi-analytical equation for three-layer CLT in current nomenclature is

$$G_{12}^*(a,a) = \frac{G_{Lt}}{1 + 3.207\rho_1^{1.2053}} \tag{34}$$

The dashed curve in Fig. 4 plots this result, which agrees better with MPM calculations. It could be made to fit better by a re-calibration to MPM results, but a drawback of the approach is that it needs numerical calibration for each new CLT structure.

An interesting application of 3D MPM modeling of $N \times N$ unit cells is to investigate the role of friction on crack surfaces. The analytical modeling does not account for friction, but MPM can model friction through contact methods (Nairn, 2013). The filled symbols in Fig. 4 show numerical results for shear modulus when the coefficient of friction between wood surfaces is $\mu = 0.3$. In the presence of friction, the shear stiffness only slightly increased. One should not expect that frictional loading would significantly ameliorate the effects of cracks on CLT shear properties.

Figure 5 compares in-plane Poisson's ratios for a CLT panel by modeling (Eq. (25) as solid lines) to 3D MPM calculations (symbols). The agreements are not as good as for moduli, but the results show that both Poisson's ratios approach zero as additional cracks are formed. Also note that Poisson's ratios for as-made CLT (at vertical dashed line) are significantly different than ratios calculated from a LPT theory that ignores cracks in the wood layers.

Figure 5 also plots moisture expansion coefficients for a CLT panel as a function of crack density (analytical modeling only using Eqs. (32) and (33), dashed curves). Both moisture expansion coefficients approach zero as additional cracks are formed. Like Poisson's ratio, moisture expansion coefficients for as-made CLT (at vertical dashed line) are significantly different than coefficients calculated from LPT theory that ignores cracks. Modeling predictions for thermal expansion coefficients would be similar.

3.2 Damage Mechanics Method and Extension to More Layers and to Bending

The above modeling was all for three-layer CLT and only for in-plane properties. Extensions of variational methods to any number of layers (McCartney, 1993, 1997) and to bending (Kim and Nairn, 2000a,b) are possible, but get complicated. For example, each additional layer adds an additional differential equation requiring solution for a system of coupled differential equations. A potential alternative is to use damage mechanics where a layer with cracks is replaced by an *effective* layer that is homogeneous but has reduced properties. Implementation of damage mechanics proceeds as follows:

1. By limiting the damage mechanics to the special case of three identical layers (*i.e.*, same number of cracks in each layer, $a = b$, and equal thickness layers, $\lambda_1 = 1/\lambda_2 = 2$), the analytical modeling for three-layer CLT properties reduces to $E_{11}(a)$, $E_{22}(a)$, $\nu_{12}(a)$, and $G_{12}(a)$, which depend only on a.
2. Equating these properties to the uncracked properties in Eq. (45) and solving for ply properties determines *effective* cracked layer properties. A laminate comprised of homogeneous layers with these effective properties has the same in-plane properties as the cracked three-layer CLT. The effective property solutions are:

$$\begin{aligned} E_L(a) &= E_{11}(a)\tfrac{2-5R'+(R')^2(2+\nu_{12}^2(a))}{(1-2R')(1-R'\nu_{12}^2(a))} & E_t(a) &= E_L(a)\tfrac{2-R'}{2R'-1} \\ \nu_{Lt}(a) &= \nu_{12}(a)\tfrac{R'}{2R'-1} & G_{Lt}(a) &= G_{12}(a) \end{aligned} \tag{35}$$

   where $R' = E_{22}(a)/E_{11}(a)$.
3. Substitute $E_L(a)$, $E_t(a)$, $\nu_{Lt}(a)$, and $G_{Lt}(a)$ back into Eq. (45) for any n to get approximate properties for a CLT panel with any number of alternating 0° and 90° layers.
4. To get approximate bending properties, substitute $E_L(a)$, $E_t(a)$, $\nu_{Lt}(a)$, and $G_{Lt}(a)$ into LPT equations for flexural properties of a cross-laminated panel with n alternating 0° and 90° layers (see Appendix 1):

$$\begin{aligned} \nu_{12}^{f0} &= \tfrac{2n^3R\nu_{Lt}}{\left(n^3-3n^2+2\right)+R\left(n^3+3n^2-2\right)} & & & \nu_{21}^{f0} &= \tfrac{2n^3R\nu_{Lt}}{\left(n^3+3n^2-2\right)+R\left(n^3-3n^2+2\right)} \\ E_{11}^{f0} &= \tfrac{E_LR\nu_{Lt}}{\nu_{21}^{f0}(1-R\nu_{Lt}^2)}(1-\nu_{12}^{f0}\nu_{21}^{f0}) & G_{12}^{f0} &= G_{Lt} & E_{22}^{f0} &= \tfrac{E_LR\nu_{Lt}}{\nu_{12}^{f0}(1-R\nu_{Lt}^2)}(1-\nu_{12}^{f0}\nu_{21}^{f0}) \end{aligned} \tag{36}$$

5. To find thermal expansion coefficients, substitute $E_L(a)$, $E_t(a)$, $\nu_{Lt}(a)$ into Eq. (7) to find effective $k_{xi}(a)$ and $k_{yi}(a)$, and use them to invert Eqs. (32) and Eqs. (33) with $\langle\phi_i\rangle = \langle\psi_i\rangle = 0$ to get:

$$\alpha_L(a) = \frac{2\alpha_1(a)\big(k_{x2}(a)-k_{y2}(a)\big)-\alpha_2(a)\big(k_{x1}(a)-k_{y1}(a)\big)}{2\big(k_{x2}(a)-k_{y2}(a)\big)-\big(k_{x1}(a)-k_{y1}(a)\big)} \tag{37}$$

$$\alpha_t(a) = \alpha_L(a) + \frac{3\big(\alpha_2(a)-\alpha_1(a)\big)}{2\big(k_{x2}(a)-k_{y2}(a)\big)-\big(k_{x1}(a)-k_{y1}(a)\big)} \tag{38}$$

6. To find moisture expansion coefficients, replace all thermal expansion coefficients (α) in the previous equations with moisture expansion coefficients (β).

Obviously, once all effective properties are known, LPT can easily find any property of any CLT structure as a function of crack spacing. A useful calculation is to find bending properties including bending properties of CLT with other arrangements of the 0° and 90° layers (*e.g.*, with more 0° layers on the surface to enhance bending stiffness in one direction). One sample calculation for bending modulus of alternating-layer CLT is shown in Fig. 6. The bending modulus with 0° plies on the surface, E_{11}^f, is much higher, as expected, then when 90° plies on on the surface (E_{22}^f). The bending modulus for these two directions get closer as the number of layers in the CLT increased from $n = 3$ to $n = 7$. Cracks in the layers have very little effect on E_{11}^f but a larger effect on E_{22}^f.

Examination of implied effective properties of the homogenized layers provides interesting results. Such calculations show which layer properties are most affected by cracks and are plotted in Fig. (7). The longitudinal modulus of the timber layers ($E_L(a)$) is essentially independent of the cracks. In contrast, all other in-plane properties ($E_t(a)$, $\nu_{tL}(a)$, and $G_{Lt}(a)$) are significantly and rapidly reduced by cracks. Even in the as-made CLT structure (at vertical dashed line), the properties are already significantly affected. The transverse moisture expansion coefficient ($\beta_t(a)$) increases while the longitudinal coefficient ($\beta_L(a)$) remains close to zero (and is not plotted).

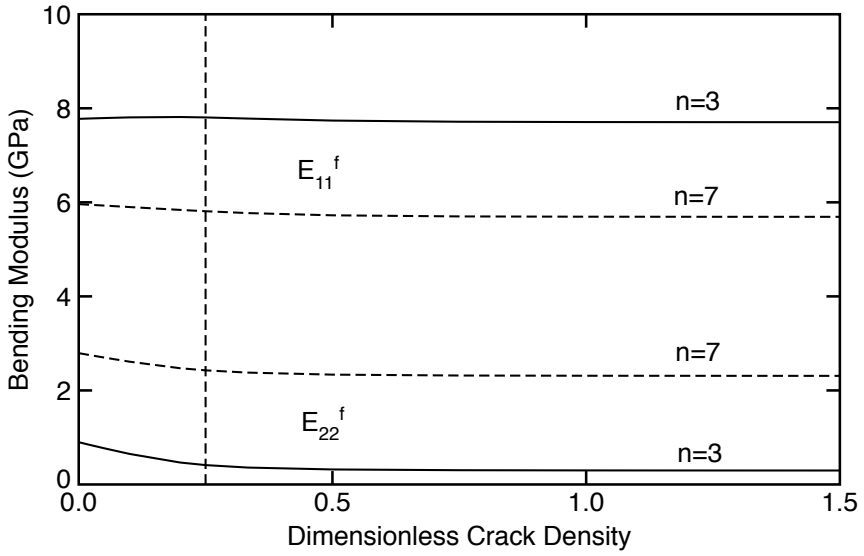

Fig. 6 The bending moduli in the two directions (E_{11}^f and E_{22}^f) for a three-layer and a seven-layer CLT panel as a function of crack density.

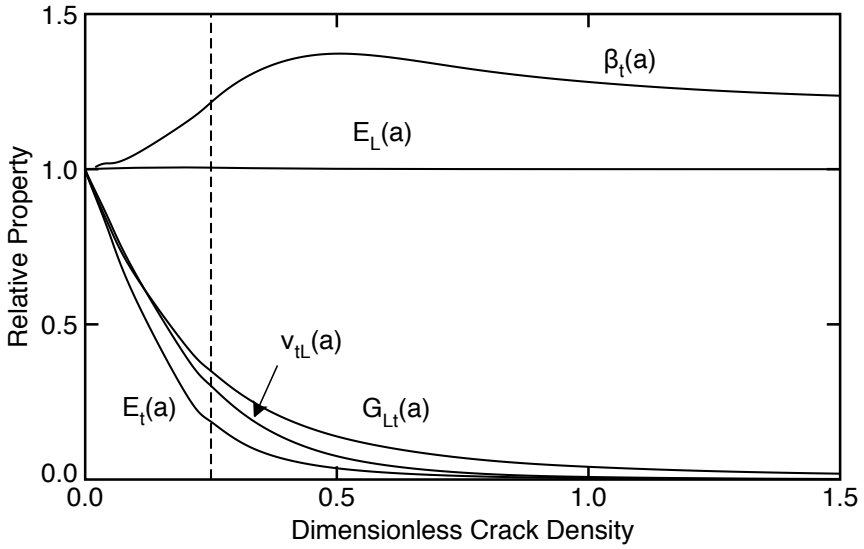

Fig. 7 The effective properties of a timber layer as a function of crack density in the layer. All properties were normalized to their value with no cracks.

3.3 Limitations

The above analysis gives results for all mechanical and expansion properties of CLT by analytical methods, but, as inevitable in 3D composite analyses, those methods needed approximations. First, variational mechanics methods minimized complementary energy, which leads to lower bound moduli. Lower bound moduli give conservative results that could be useful in design. But, if the lower bounds are too pessimistic, those conservative numbers would result in over-designed structures. The comparisons to numerical modeling shows that tensile moduli are accurate or that the lower bound is a "tight" bound on actual CLT properties. In contrast, the lower bound shear modulus is farther from numerical results. Because shear stiffness of CLT panels is an important property, the derivation of improved shear modulus predictions is desirable.

Second, the boundary conditions used to solve the variational mechanics equations model all crack surfaces as stress free (see Eq. (8)). These conditions are most appropriate for tensile loading. If compression loading, however, causes sufficient deformation to close gaps and cracks in the layers, those crack surfaces may transmit normal stress and, through friction, may transmit shear stress. In other words, the problem is non-linear. The results here give linear results for tensile loading, while the compression results may be higher. Still, the tensile results can provide conservative design guides for all loading conditions. Numerical results on the effect of friction on shear modulus (see Fig. 4), show that crack contact does not significantly enhance shear properties. When CLT designs are dominated by compression loading with little shear or tension, one could hope that stress transfer at crack surfaces would contribute to integrity and durability of that structure. But doing so risks comparison to a "house of cards" (*i.e.*, a structure held up by contact and friction alone).

Extension to more than three layers and too bending relied on effective property methods. Although such methods are common in laminate analysis, they are an approximation. Replacing a cracked ply with a homogeneous ply with reduced properties may work in an averaged sense, but cannot capture effects of local stress concentrations at crack tips. The effective properties were deduced from the $n = 3$ solutions. To use those properties in other laminates, the damage mechanics had to assume that effective properties are independent of the number of layers in the panel and of location the layer in the panel. To calculate bending properties, the damage mechanics had to assume that effective properties are the same for layers in tension and compression. As discussed above, this approach may be good for layers in tension, but may underestimate properties of layers in compression due to crack contact. Despite these limitations, the damage mechanics approach still provides a rational approach for investigating the role of cracks on all CLT properties.

Finding bending properties using LPT is an application of simple plate theory that ignores role of transverse shear on displacements. This approach works well for thin panels, but CLT panels are typically much thicker than other wood panels. The modeling of shear effects on bending could follow by analysis of $G_{23}(a,b)$ and $G_{13}(a,b)$, but these two shear properties were not covered in this paper and I am unaware of any results in the composites literature. If found, bending analysis of anisotropic laminates shows that the magnitude of the shear effect for the two bending directions would scale with $E_{11}(a,b)/G_{13}(a,b)$ and $E_{22}(a,b)/G_{23}(a,b)$. Because these ratios are typically high and because $G_{23}(a,b)$ and $G_{13}(a,b)$ are reduced by the low rolling shear modulus of the transverse layers, the shear effects on bending should be a concern.

This modeling did not address quality of adhesion along the glued timbers faces between layers. This bonding was assumed to be perfect such that displacements between layers are equal at layer interfaces. If glue is inadequately spread on the faces, if glue is more compliant than the wood, or if thickness variations among the boards inhibits adequate contact during pressing, the adhesive bonds may be less than perfect. To the extent that bond lines can slip (due to delamination or compliant glue), analyses that assume perfect bonding overestimate stiffness properties. This issue can be addressed by either laminate damage mechanics that accounts for interfacial slip (*e.g.*, Allen (1994)) or by modeling bond lines as imperfect interfaces (Hashin, 1990, 1992).

Finally, this work analyzed the consequence of cracks, but does not address the speed at which additional cracks form. This information is crucial to durability analysis of CLT panels. Experience from microcracking of cross-laminated composites shows that crack formation is best studied by a combination of experiments and fracture mechanics modeling (Nairn and Hu, 1994; Nairn, 2000; Nairn et al, 1993). The experiments observe crack formation due to mechanical loads or to changes in temperature and moisture content. Observations of crack density as a function of loading are then interpreted assuming the next crack forms when the energy released by that crack exceeds the *in situ* toughness of the timber. The calculation of released energy can be reduced to finding changes in mechanical and expansion properties. The results in this paper, therefore, providing a starting point for recommended work on cracking of CLT panels.

4 Conclusions

This paper describes variational mechanics analysis of a three layer CLT panel. The analytical solutions give all in-plane mechanical and expansion properties. The moduli are lower bound moduli; the tensile moduli appear to be very tight bounds, but the shear modulus is more pessimistic. By using the three-layer theory to deduce *effective* layer properties as a function of the number of cracks, the analysis can be extended to bending properties and to CLT panels with any number or arrangement of layers. Future modeling may improve on these results by deriving improved shear analysis and by accounting for crack contact during compression loading. The more important issue,

however, is understanding the rate at which CLT panels form additional cracks. This understanding could lead either to re-design of CLT panels to minimize cracking or to improved design of CLT structures that accounts for appearance of those cracks. This paper's results provided input for the recommended fracture mechanics experiments on CLT layer cracking.

Acknowledgements This work was made possible by the endowment for the Richardson Chair in Wood Science and Forest Products.

Appendix 1

This appendix gives minimal, yet complete, laminated plate theory (LPT) equations for symmetric cross-laminated materials. Consider a n-layer laminate where each layer has the same thickness $t^{(k)}$. The z axis is in the thickness direction with $z=0$ in the middle of the laminate and total thickness is h. The force (N_{ij}) and moment (M_{ij}) resultants are given by:

$$\begin{pmatrix} N_{11} \\ N_{22} \\ N_{12} \end{pmatrix} = \begin{bmatrix} A_{11} & A_{12} & A_{16} \\ A_{12} & A_{22} & A_{26} \\ A_{16} & A_{26} & A_{66} \end{bmatrix} \begin{pmatrix} \varepsilon^0_{11} \\ \varepsilon^0_{22} \\ \gamma^0_{12} \end{pmatrix} \text{ and } \begin{pmatrix} M_{11} \\ M_{22} \\ M_{12} \end{pmatrix} = \begin{bmatrix} D_{11} & D_{12} & D_{16} \\ D_{12} & D_{22} & D_{26} \\ D_{16} & D_{26} & D_{66} \end{bmatrix} \begin{pmatrix} \kappa_{11} \\ \kappa_{22} \\ \kappa_{12} \end{pmatrix} \tag{39}$$

where ε^0_{ij} and κ_{ij} are in-plane strains and curvatures applied to the laminate, and

$$A_{ij} = \sum_{k=1}^{n} Q^{(k)}_{ij} t^{(k)} \quad \text{and} \quad D_{ij} = \sum_{k=1}^{n} Q^{(k)}_{ij} t^{(k)} \left({z^{(k)}_{mid}}^2 + \frac{{t^{(k)}}^2}{12} \right) \tag{40}$$

where $Q^{(k)}_{ij}$ are elements of the plane-stress stiffness matrix for layer k and $z^{(k)}_{mid}$ is the layer's midpoint. A cross laminated material is divided into 0° layers (wood grain in the 1 direction) and 90° layers (wood grain in the 2 direction). In 0° layers, the non-zero stiffnesses are $Q^{(0)}_{11} = E_L/(1-R\nu^2_{Lt})$, $Q^{(0)}_{22} = RQ^{(0)}_{11}$, $Q^{(0)}_{12} = R\nu_{Lt}Q^{(0)}_{11}$, and $Q^{(0)}_{66} = G_{Lt}$, where E_L and G_{Lt} are longitudinal and shear stiffness of the layers, ν_{Lt} is axial Poisson's ratio, and $R = E_t/E_L$ is ratio of transverse to longitudinal stiffness. The stiffnesses for 90° layers are the same except $Q^{(90)}_{11} = Q^{(0)}_{11}$ and $Q^{(90)}_{22} = Q^{(0)}_{22}$ are switched. The resulting non-zero LPT terms are

$$\begin{array}{cccc} A_{11} = hQ^{(0)}_{11}(V_0 + RV_{90}) & A_{22} = hQ^{(0)}_{11}(V_{90} + RV_0) & A_{12} = hR\nu_{Lt}Q^{(0)}_{11} & A_{66} = hG_{Lt} \\ D_{11} = \frac{h^3 Q^{(0)}_{11}}{12}(V_0 I_0 + RV_{90} I_{90}) & D_{22} = \frac{h^3 Q^{(0)}_{11}}{12}(V_{90} I_{90} + RV_0 I_0) & D_{12} = \frac{h^3 R\nu_{Lt} Q^{(0)}_{11}}{12} & D_{66} = \frac{h^3 G_{Lt}}{12} \end{array} \tag{41}$$

where V_0 and V_{90} are volume fractions of 0° and 90° plies,

$$I_0 = \left(\frac{t}{h}\right)^2 \left(1 + \frac{12}{htV_0} \sum_{0^\circ \text{ plies}} {z^{(k)}_{mid}}^2 \right), \quad \text{and} \quad I_{90} = \frac{1 - V_0 I_0}{V_{90}} \tag{42}$$

These results assume all layers have the same thickness t and identical properties. Generalization to varying thicknesses or properties is easy. To find mechanical properties, the $[A]$ and $[D]$ matrices are inverted and compared to an effective compliance matrix. Explicit results for all non-zero in plane and flexural properties are:

$$\begin{array}{ccc} \nu^0_{12} = \frac{A_{12}}{A_{22}} = \frac{R\nu_{Lt}}{V_{90}+RV_0} & \nu^0_{21} = \frac{A_{12}}{A_{11}} = \frac{R\nu_{Lt}}{V_0+RV_{90}} & G^0_{12} = \frac{A_{66}}{h} = G_{Lt} \\ E^0_{11} = \frac{A_{11}}{h}(1-\nu^0_{12}\nu^0_{21}) = \frac{Q^{(0)}_{11} R\nu_{Lt}}{\nu^0_{21}}(1-\nu^0_{12}\nu^0_{21}) & & E^0_{22} = \frac{\nu^0_{21} E^0_{11}}{\nu^0_{12}} \\ \nu^{f0}_{12} = \frac{D_{12}}{D_{22}} = \frac{R\nu_{Lt}}{V_{90}I_{90}+RV_0I_0} & \nu^{f0}_{21} = \frac{D_{12}}{D_{11}} = \frac{R\nu_{Lt}}{V_0 I_0+RV_{90}I_{90}} & G^{f0}_{12} = \frac{12D_{66}}{h^3} = G_{Lt} \\ E^{f0}_{11} = \frac{12D_{11}}{h^3}(1-\nu^{f0}_{12}\nu^{f0}_{21}) = \frac{Q^{(0)}_{11} R\nu_{Lt}}{\nu^{f0}_{21}}(1-\nu^{f0}_{12}\nu^{f0}_{21}) & & E^{f0}_{22} = \frac{\nu^{f0}_{21} E^{f0}_{11}}{\nu^{f0}_{12}} \end{array} \tag{43}$$

The above results are general for any symmetric, cross-ply laminate. If the laminate additionally has n (an odd number) alternating layers (which is appropriate for most CLT as well as for plywood), we can reduce the above using:

$$V_0 = \frac{1}{2} + \frac{1}{2n}, \quad V_{90} = \frac{1}{2} - \frac{1}{2n}, \quad V_0 I_0 = (n^3 + 3n^2 - 2)/(2n^3), \quad \text{and} \quad V_{90} I_{90} = 1 - V_0 I_0 \tag{44}$$

to get in-plane properties of

$$\begin{array}{ccc} \nu_{12}^0 = \frac{2nR\nu_{Lt}}{(n-1)+R(n+1)} & & \nu_{21}^0 = \frac{2nR\nu_{Lt}}{(n+1)+R(n-1)} \\ E_{11}^0 = \frac{E_L R\nu_{Lt}}{\nu_{21}^0(1-R\nu_{Lt}^2)}(1-\nu_{12}^0\nu_{21}^0) & G_{12}^0 = G_{Lt} & E_{22}^0 = \frac{E_L R\nu_{Lt}}{\nu_{12}^0(1-R\nu_{Lt}^2)}(1-\nu_{12}^0\nu_{21}^0) \end{array} \tag{45}$$

and bending properties of

$$\begin{array}{ccc} \nu_{12}^{f0} = \frac{2n^3R\nu_{Lt}}{\left(n^3-3n^2+2\right)+R\left(n^3+3n^2-2\right)} & & \nu_{21}^{f0} = \frac{2n^3R\nu_{Lt}}{\left(n^3+3n^2-2\right)+R\left(n^3-3n^2+2\right)} \\ E_{11}^{f0} = \frac{E_L R\nu_{Lt}}{\nu_{21}^{f0}(1-R\nu_{Lt}^2)}(1-\nu_{12}^{f0}\nu_{21}^{f0}) & G_{12}^{f0} = G_{Lt} & E_{22}^{f0} = \frac{E_L R\nu_{Lt}}{\nu_{12}^{f0}(1-R\nu_{Lt}^2)}(1-\nu_{12}^{f0}\nu_{21}^{f0}) \end{array} \tag{46}$$

These results are used in text of the paper for baseline CLT properties and in *effective* property equations for cracked CLT panels.

Appendix 2

Analysis of cross-laminated timber (CLT) properties in the two loading directions can be reduced to a complementary energy identical to Hashin (1987) except using different constants (see Eq. (10) in text of paper). The constants relevant for loading CLT in the $i = 1$ direction are:

$$\begin{array}{ccc} A_0 = \frac{1}{E_t} + \frac{1}{\lambda_i E_L} & B_0 = -\frac{\nu_{Lt}(1+\lambda_i)}{\lambda_i E_L} & C_0 = \frac{1}{E_L} + \frac{1}{\lambda_i E_t} \\ A_1 = \frac{1}{3G_{RS}} + \frac{\lambda_i}{3G_{Lr}} & B_1 = \frac{1}{3G_{Lr}} + \frac{\lambda_i}{3G_{RS}} & A_2 = \frac{(3\lambda_1+2)\nu_{tr}}{3E_t} - \frac{\lambda_1\nu_{Lr}}{3E_L} \\ B_2 = \frac{(3\lambda_1+2)\nu_{Lr}}{3E_L} - \frac{\lambda_1\nu_{tr}}{3E_t} & C_2 = \frac{(\lambda_1+1)(3\lambda_1^2+12\lambda_1+8)}{60E_r} & \end{array} \tag{47}$$

For loading in the 2 direction, use $i = 2$ in first five constants and replace the last three constants with:

$$A_2' = \frac{(2\lambda_2+3)\nu_{Lr}}{3E_L} - \frac{\nu_{tr}}{3E_t} \quad B_2' = \frac{(2\lambda_2+3)\nu_{tr}}{3E_t} - \frac{\nu_{Lr}}{3E_L} \quad C_2' = \frac{(\lambda_2+1)(8\lambda_2^2+12\lambda_2+3)}{60E_r} \tag{48}$$

Also note that because $\lambda_2 = 1/\lambda_1$, the direction 2 constants (primed) can be expressed in terms of direction 1 constants using:

$$A_0' = \lambda_1 C_0,\ B_0' = \lambda_1 B_0,\ C_0' = \lambda_1 A_0,\ A_1' = \frac{B_1}{\lambda_1}, B_1' = \frac{A_1}{\lambda_1},\ A_2' = \frac{B_2}{\lambda_1},\ B_2' = \frac{A_2}{\lambda_1}.\ C_2' = \frac{C_2}{\lambda_1^3} \tag{49}$$

Using the calculus of variations to minimize complementary energy in Eq. (10) of the paper text, the $\phi_i(\xi)$ and $\psi_i(\xi)$ functions can be determined by solving two coupled, fourth-order differential equations (Hashin, 1987):

$$\frac{d^4\phi_i(\xi)}{d\xi^4} + p_1\frac{d^2\phi_i(\xi)}{d\xi^2} + q_1\phi(\xi) + \frac{k_{yi}}{k_{xi}}\frac{B_0}{C_2}\langle\psi_i\rangle = 0 \tag{50}$$

$$\frac{d^4\psi_i(\eta)}{d\eta^4} + p_2\frac{d^2\psi_i(\eta)}{d\eta^2} + q_2\psi(\eta) + \frac{k_{xi}}{k_{yi}}\frac{B_0}{C_2}\langle\phi_i\rangle = 0 \tag{51}$$

where

$$p_1 = \frac{A_2 - A_1}{C_2}, \quad q_1 = \frac{A_0}{C_2}, \quad p_2 = \frac{B_2 - B_1}{C_2} \quad \text{and} \quad q_2 = \frac{C_0}{C_2} \tag{52}$$

but A_2, B_2, and C_2 are replaced by A_2', B_2', and C_2' for $i = 2$. The averaged values are given by

$$\langle\phi_i\rangle = \frac{1}{2\rho_i}\int_{-\rho_i}^{\rho_i}\phi_i(\xi)\,d\xi \qquad \text{and} \qquad \langle\psi_i\rangle = \frac{1}{2\chi_i}\int_{-\chi_i}^{\chi_i}\psi_i(\eta)\,d\eta \tag{53}$$

Note some nomenclature differences from Hashin (1987): ρ_1 and ρ_2 in Hashin (1987) are replaced here by ρ_i and χ_i. The terms ρ_2 and χ_2 here are new terms for solving loading direction $i = 2$, which was not considered in Hashin (1987).

All combinations of CLT properties have $p_1 < 0$ and $q_1 > 0$. When $4q_1 > p_1^2$, the solution for $\phi_i(\xi)$, which satisfies its differential equation and boundary conditions, is:

$$\phi_i(\xi) = \big(1 + m_{i,1}\langle\psi_i\rangle\big)\big(D_1\cosh(\alpha\xi)\cos(\beta\xi) + D_2\sinh(\alpha\xi)\sin(\beta\xi)\big) - m_{i,1}\langle\psi_i\rangle \tag{54}$$

where $\alpha,\beta = \frac{1}{2}\sqrt{2\sqrt{q_1} \mp p_1}$ and

$$D_1 = \frac{2\big(\alpha\cosh(\alpha\rho_i)\sin(\beta\rho_i) + \beta\sinh(\alpha\rho_i)\cos(\beta\rho_i)\big)}{\beta\sinh(2\alpha\rho_i) + \alpha\sin(2\beta\rho_i)} \tag{55}$$

$$D_2 = \frac{2\big(\beta\cosh(\alpha\rho_i)\sin(\beta\rho_i) - \alpha\sinh(\alpha\rho_i)\cos(\beta\rho_i)\big)}{\beta\sinh(2\alpha\rho_i) + \alpha\sin(2\beta\rho_i)} \tag{56}$$

$$m_{i,1} = \frac{k_{yi}}{k_{xi}}\frac{B_0}{A_0} \tag{57}$$

The average value of $\phi_i(\xi)$ is

$$\langle\phi_i\rangle = \big(1 + m_{i,1}\langle\psi_i\rangle\big)\omega_1 - m_{i,1}\langle\psi_i\rangle \tag{58}$$

where

$$\omega_1 = \frac{2\alpha\beta\big(\cosh(2\alpha\rho_i) - \cos(2\beta\rho_i)\big)}{\rho_i(\alpha^2+\beta^2)\big(\beta\sinh(2\alpha\rho_i) + \alpha\sin(2\beta\rho_i)\big)} \tag{59}$$

When $4q_1 < p_1^2$, the solution for $\phi_i(\xi)$ is:

$$\phi_i(\xi) = \big(1 + m_{i,1}\langle\psi_1\rangle\big)\big(D_1\cosh(\alpha\xi) + D_2\cosh(\beta\xi)\big) - m_{i,1}\langle\psi_i\rangle \tag{60}$$

where $\alpha,\beta = \sqrt{-(p_1/2) \pm \sqrt{(p_1^2/4) - q_1}}$ and

$$D_1 = -\frac{\beta\sinh(\beta\rho_i)}{\alpha\sinh(\alpha\rho_i)\cosh(\beta\rho_i) - \beta\cosh(\alpha\rho_1)\sinh(\beta\rho_i)} \tag{61}$$

$$D_2 = \frac{\alpha\sinh(\alpha\rho_i)}{\alpha\sinh(\alpha\rho_i)\cosh(\beta\rho_i) - \beta\cosh(\alpha\rho_1)\sinh(\beta\rho_i)} \tag{62}$$

The average value of $\phi_i(\xi)$ is identical to Eq. (58), except now

$$\omega_1 = \frac{(\alpha^2-\beta^2)\sinh(\alpha\rho_i)\sinh(\beta\rho_i)}{\rho_i\alpha\beta\big(\alpha\sinh(\alpha\rho_i)\cosh(\beta\rho_i) - \beta\cosh(\alpha\rho_i)\sinh(\beta\rho_i)\big)} \tag{63}$$

To find $\psi_i(\eta)$, use the above equations but replace $\phi_i(\xi)$, p_1, q_1, ρ_i, $m_{i,1}$, $\langle\psi_i\rangle$, ω_1, and ξ with $\psi_i(\eta)$, p_2, q_2, χ_i, $m_{i,2} = k_{xi}B_0/(k_{yi}C_0)$, $\langle\phi_i\rangle$, ω_2, and η, respectively, and note that α and β will be different.

All effective properties depend on the average values $\langle\phi_i\rangle$ and $\langle\psi_i\rangle$. To find these terms, solve Eq. (58) and the corresponding equation for $\langle\psi_i\rangle$ to get:

$$\langle\phi_i\rangle = \frac{\omega_1 - m_{i,1}\omega_2(1-\omega_1)}{1 - m_{i,1}m_{i,2}(1-\omega_1)(1-\omega_2)} \qquad \text{and} \qquad \langle\psi_i\rangle = \frac{\omega_2 - m_{i,2}\omega_1(1-\omega_2)}{1 - m_{i,1}m_{i,2}(1-\omega_1)(1-\omega_2)} \tag{64}$$

where ω_1 and ω_2 are determined from the appropriate form for $\phi_i(\xi)$ and $\psi_i(\eta)$ in the previous equations. Repeating this calculation for both loading directions determines all CLT mechanical properties.

Appendix 3

The results for both directions are expressible from equations in Appendix 2, but can be clarified in terms of a single dimensionless function and a single set of constants. The new function is $\Omega(\rho,p,q)$ with the single case in previous section defining the function by:

$$\Omega(\rho=\rho_i,p=p_1,q=q_1)=\omega_1(\rho_i,p_1,q_1) \tag{65}$$

Then for loading in the $i=1$ direction:

$$\langle\phi_1\rangle=\frac{\omega_1-m_{1,1}\omega_2(1-\omega_1)}{1-m_{1,1}m_{1,2}(1-\omega_1)(1-\omega_2)} \qquad \text{and} \qquad \langle\psi_1\rangle=\frac{\omega_2-m_{1,2}\omega_1(1-\omega_2)}{1-m_{1,1}m_{1,2}(1-\omega_1)(1-\omega_2)} \tag{66}$$

where

$$\omega_1=\Omega\left(\rho_a,\frac{A_2-A_1}{C_2},\frac{A_0}{C_2}\right) \quad \text{and} \quad \omega_2=\Omega\left(\rho_b,\frac{B_2-B_1}{C_2},\frac{C_0}{C_2}\right) \tag{67}$$

with $\rho_a=a/t_1$ and $\rho_b=b/t_1$. For loading in the $i=2$ direction:

$$\langle\phi_2\rangle=\frac{\omega_1'-m_{2,1}\omega_2'(1-\omega_1')}{1-m_{2,1}m_{2,2}(1-\omega_1')(1-\omega_2')} \qquad \text{and} \qquad \langle\psi_2\rangle=\frac{\omega_2'-m_{2,2}\omega_1'(1-\omega_2')}{1-m_{2,1}m_{2,2}(1-\omega_1')(1-\omega_2')} \tag{68}$$

where

$$\omega_1'=\Omega\left(\frac{\rho_b}{\lambda},\lambda^2\frac{B_2-B_1}{C_2},\lambda^4\frac{C_0}{C_2}\right) \quad \text{and} \quad \omega_2'=\Omega\left(\frac{\rho_a}{\lambda},\lambda^2\frac{A_2-A_1}{C_2},\lambda^4\frac{A_0}{C_2}\right) \tag{69}$$

with $\lambda=\lambda_1$.

References

Allen DH (1994) Damage evolution in laminates. In: Talreja R (ed) Damage Mechanics of Composite Materials, Elsevier, Amsterdam, pp 79–116

Bogensperger T, Moosbrugger T, Silly G (2010) Verification of clt-plates under loads in plane. In: World Conference on Timber Engineering, Riva del Garda, Italy, pp June 20–24

Christenson RM (1979) Mechanics of Composite Materials. John Wiley & Sons, New York

Frost SR (1994) The impact behaviour and damage tolerance of filament would glass fibre/epoxy matrix pipes. In: 6^{th} Int'l Conf. of Fiber-Reinforced Composites, University of Newcastle upon Tyne, March 29-31, vol 3, pp 1–10

Gibson LJ, Ashby MF (1997) Cellular Solids: Structure and Properties. Cambridge University Press, Cambridge, England

Hashin Z (1985) Analysis of cracked laminates: A variational approach. Mech of Mat 4:121–136

Hashin Z (1986) Analysis of stiffness reduction of cracked cross-ply laminates. Eng Fract Mech 25:771–778

Hashin Z (1987) Analysis of orthogonally cracked laminates under tension. J Appl Mech 54:872–879

Hashin Z (1988) Thermal expansion coefficients of cracked laminates. Comp Sci & Tech 31:247–260

Hashin Z (1990) Thermoelastic properties of fiber composites with imperfect interface. Mech of Materials 8:333–348

Hashin Z (1992) Extremum principles for elastic heterogenous media with imperfect interfaces and their application to bounding of effective moduli. Journal of the Mechanics and Physics of Solids 40(4):767–781

Hashin Z (2010) Shear modulus of orthongally crack laminates, personal communication

Jones RM (1975) Mechanics of Composite Materials. Scripta Book Company, Washington, DC

Kim SR, Nairn JA (2000a) Fracture mechanics analysis of coating/substrate systems subjected to tension or bending loads I: Theory. Engr Fract Mech 65:573–593

Kim SR, Nairn JA (2000b) Fracture mechanics analysis of coating/substrate systems subjected to tension or bending loads II: Experiments in bending. Engr Fract Mech 65:595–607

Levin VM (1967) On the coefficients of thermal expansion in heterogeneous materials. Mechanics of Solids 2:58–61

McCartney LN (1993) Stress transfer mechanics for multiple perfectly bonded concentric cylinder models of unidirectional composites. National Physical Lab Report DMM(A)129

McCartney LN (1997) Predicting steady state delamination in a cross-ply laminate subject to through-thickness pressure. NPL Report CMMT(A) 65

Nairn JA (1989) The strain energy release rate of composite microcracking: A variational approach. J Comp Mat 23:1106–1129

Nairn JA (2000) Matrix microcracking in composites. In: Talreja R, Manson JAE (eds) Comprehensive Composite Materials, vol 2, Elsevier Science, pp 403–432

Nairn JA (2007) A numerical study of the transverse modulus of wood as a function of grain orientation and properties. Holzforschung 61:406–413

Nairn JA (2013) Modeling of imperfect interfaces in the material point method using multimaterial methods. Computer Modeling in Eng & Sci 92(3):271–299

Nairn JA (2016a) Material point method (NairnMPM) and finite element analysis (NairnFEA) open-source software. http://osupdocs.forestry.oregonstate.edu/index.php/Main_Page

Nairn JA (2016b) Mechanical properties of cross-laminated timber accounting for non-bonded edges and additional cracks. In: World Conference on Timber Engineering, Vienna, Austria, pp August 22–25

Nairn JA, Hu S (1994) Micromechanics of damage: A case study of matrix microcracking. In: Talreja R (ed) Damage Mechanics of Composite Materials, Elsevier, Amsterdam, pp 187–243

Nairn JA, Hu S, Bark JS (1993) A critical evaluation of theories for predicting microcracking in composite laminates. J Mat Sci 28:5099–5111

Parvizi A, Garrett KW, Bailey JE (1978) Constrained cracking in glass fiber-reinforced epoxy cross-ply laminates. J Mat Sci 13:195–201

Sulsky D, Chen Z, Schreyer HL (1994) A particle method for history-dependent materials. Comput Methods Appl Mech Engrg 118:179–186